JACC: CARDIOVASCULAR IMAGING VOL. 4, NO. 6, 2011

ISSN 1936-878X/$36.00
PUBLISHED BY ELSEVIER INC. DOI:10.1016/j.jcmg.2011.03.014

Plaque Characteristics of Thin-Cap Fibroatheroma Evaluated by OCT and IVUS

Yoshinori Miyamoto, MD, Hiroyuki Okura, MD, Teruyoshi Kume, MD, Takahiro Kawamoto, MD, Yoji Neishi, MD, Akihiro Hayashida, MD, Ryotaro Yamada, MD, Koichiro Imai, MD, Ken Saito, MD, Kiyoshi Yoshida, MD

Kurashiki, Japan

OBJECTIVES The purpose of this study was to assess plaque characteristics of optical coherence tomography (OCT)-derived thin-cap fibroatheroma (TCFA) by integrated backscatter intravascular ultrasound (IB-IVUS).

BACKGROUND Radiofrequency signal-derived IVUS tissue characterization technology has become clinically available and provided objective and quantitative plaque characteristics of the coronary vessel wall. Integrated backscatter IVUS is one of the tissue characterization methods that can possibly provide quantitative plaque characteristics of the OCT-derived TCFA.

METHODS Eighty-one coronary lesions with plaque burden >40% were selected and analyzed with both IB-IVUS and OCT. The OCT-derived TCFA was defined as a presence of thin fibrous cap (<65 μm) overlying a signal-poor lesion with diffuse border representing a lipid-rich plaque. By conventional gray-scale IVUS, external elastic membrane (EEM) cross-sectional area (CSA), lumen CSA, plaque plus media (P+M) CSA, plaque burden and remodeling index were measured. By IB-IVUS, plaque characteristics were further classified as fibrosis, dense fibrosis, calcification, or lipid pool.

RESULTS Optical coherence tomography identified 40 TCFAs (49%) and 41 non-TCFAs. The EEM CSA, P+M CSA, plaque burden, and remodeling index were significantly larger in OCT-derived TCFA than non-TCFA. By IB-IVUS, percentage lipid pool area (= lipid pool area/P+M CSA × 100) was significantly higher (62.4 ± 12.8% vs. 38.4 ± 13.1%, $p < 0.0001$) and percentage fibrosis area (= fibrosis area/P+M CSA × 100) was significantly lower (34.6 ± 11.4% vs. 50.5 ± 8.7%, $p < 0.0001$) in OCT-derived TCFA than non-TCFA. By receiver-operator characteristic curve analysis, percentage lipid pool area ≥55%, percentage fibrosis area ≤41%, and remodeling index ≥1.0 were predictors of OCT-derived TCFA.

CONCLUSIONS The OCT-derived TCFA had larger plaque burden and positive remodeling with predominant lipid component and less fibrous plaque assessed by IB-IVUS. (J Am Coll Cardiol Img 2011;4:638–46) © 2011 by the American College of Cardiology Foundation

From the Department of Cardiology, Kawasaki Medical School, Kurashiki, Japan. This research was partially supported by the Japanese Ministry of Education, Culture, Sports, Science and Technology, Grant-in-Aid for Scientific Research (No. 20590849). All authors have reported that they have no relationships to disclose.

Manuscript received November 14, 2010; revised manuscript received March 2, 2011, accepted March 10, 2011.

Studies conducted over the past 15 years have demonstrated that even minimally or moderately stenotic atherosclerotic plaques can cause acute myocardial infarction and sudden cardiac death. Because plaque characteristics of the vulnerable plaque (i.e. thin-cap fibroatheroma [TCFA]) are microstructural, diagnostic technique requires high spatial (axial, lateral, elevational) and temporal resolution. Pathologically, TCFAs are characterized as a presence of a large lipid pool with overlying thin fibrous cap (<65 μm) (1). Although

See page 656

intravascular ultrasound (IVUS) is widely used to visualize coronary arteries in the clinical setting, its resolution (100 to 150 μm) is not high enough to identify presence of thin-fibrous cap. Intracoronary optical coherence tomography (OCT) has been introduced as an alternative intracoronary imaging technology, providing better resolution (10 to 20 μm) than IVUS (2). It has been reported that OCT could measure the thickness of the fibrous cap and thus reliably detect TCFA (3,4). By contrast, because OCT has a limited depth of penetration (5), it is difficult to visualize the entire plaque structure and to quantitatively assess plaque characteristics.

Recently, radiofrequency (RF) signal-derived IVUS tissue characterization technology has become clinically available and provided objective and quantitative plaque characteristics of the coronary vessel wall. Integrated backscatter intravascular ultrasound (IB-IVUS) is one of the tissue characterization methods that can possibly predict OCT-derived TCFA and provide quantitative plaque characteristics of the OCT-derived TCFA. We hypothesized that IB-IVUS could provide quantitative plaque characteristics of the OCT-derived TCFA. Therefore, the purpose of this study was to evaluate OCT-derived TCFA and to investigate plaque characteristics of the OCT-derived TCFA with gray-scale IVUS and IB-IVUS.

METHODS

Study population. Between April 2007 and November 2009, 141 consecutive patients who underwent both OCT and IVUS imaging were enrolled and studied. Lesion inclusion criteria were: 1) de novo lesion; and 2) lesions with plaque burden >40% assessed by IVUS (1,6,7). Thus, of the 141 patients, 61 patients who did not have coronary artery lesions with plaque burden >40% by IVUS were not included. Patients with poor OCT/IVUS image quality (n = 12), ostial lesion (n = 2), severely (>180°) calcified lesion (n = 5), and lesion with thrombus (n = 5) were excluded. Finally, 56 patients with coronary artery disease (46 stable angina pectoris, 10 acute coronary syndrome [ACS]) were enrolled in this study. The OCT-derived TCFA was defined as a presence of thin fibrous cap (<65 μm) overlying a signal-poor lesion (>90°) with diffuse border representing a lipid-rich plaque (8). Plaque with thick fibrous cap (≥65 μm) was defined as non-TCFA.

IVUS and OCT imaging. A commercially available IVUS imaging system (Galaxy 2, Boston Scientific, Natick, Massachusetts) and an IVUS catheter (Atlantis SR Pro 2.5-F, 40-MHz, Boston Scientific) were used. A commercially available personal computer with custom software (IB-IVUS, YD Co., Ltd., Nara, Japan) was connected to the IVUS imaging system to obtain RF signal for subsequent analysis. All patients received heparin (100 U/kg), and the IVUS catheter was inserted into the coronary artery through a 6- to 7-F coronary guiding catheter over a 0.014-inch guidewire. To prevent coronary spasm, nitroglycerin (200 μg) or isosorbide dinitrate (1 mg) was injected before any imaging procedures. The transducer was pulled back automatically at 0.5 mm/s to obtain the imaging sequence, which started at least 10 mm distal to plaque being analyzed. A single frame of each IB-IVUS image was divided into picture elements (minimum units for evaluation of IB-value) in the following sequence: 1) the image was divided into 256 vector lines (1.4 grade/line); and 2) 71 regions of interest were defined for each 50-μm depth on each vector line. Accordingly, volumetric elements were expressed approximately as $2\pi r/256 \times 0.05$ mm $\times$ 1.0 mm (r = distance from the center of IVUS catheter). The IB values were calculated as the average power of the ultrasound backscattered signals from a small volume of tissue. For that purpose, fast Fourier transform was used and measured in decibels (dB). It was reported that the attenuation for the distance from lumen-intima border to media-adventitia border with a 40-MHz frequency catheter was 5.9 dB/mm. Therefore, we corrected each IB value by adding 0.59 dB/0.1 mm (9–11). After the IVUS procedure, OCT examination was performed as previously described (12). Briefly, an over-the-wire type occlusion balloon

ABBREVIATIONS AND ACRONYMS

2D = 2-dimensional
ACS = acute coronary syndrome
CSA = cross-sectional area
EEM = external elastic membrane
IB-IVUS = integrated backscatter intravascular ultrasound
MLA = minimal lumen area
OCT = optical coherence tomography
RF = radiofrequency
ROC = receiver-operator characteristic
TCFA = thin-cap fibroatheroma
VH = virtual histology

JACC: CARDIOVASCULAR IMAGING, VOL. 4, NO. 6, 2011
JUNE 2011:638–46

catheter (Helios, Light-Lab Imaging, Inc., Westford, Massachusetts) and a guidewire-based OCT imaging catheter (ImageWire, Light-Lab Imaging, Inc.) were inserted into the coronary artery. The OCT pullback imaging was performed with an automated pullback device (1 mm/s) from at least 10 mm distal to plaque. After occlusion of the proximal part of each coronary artery, OCT imaging was performed under continuous infusion of the lactate linger solution. Obtained OCT images were recorded on a CD-ROM for offline analysis, for which proprietary software from LightLab Imaging was used. The IVUS and OCT imaging were performed at the culprit vessel as well as nonculprit vessels.

Quantitative coronary angiography. Quantitative coronary angiography analysis was performed with the CAAS II system (Pie Medical Imaging, Maastricht, the Netherlands).

Gray-scale IVUS and IB-IVUS measurements. Each gray-scale IVUS and IB-IVUS parameter was measured. Quantitative IVUS measurements were performed at the lesion, and both proximal and distal reference were performed by an experienced IVUS analyst with commercially available planimetry software (echoPlaque 3.0 INDEC Medical Systems, Santa Clara, California). Cross-sectional images were quantified for lumen cross-sectional area (CSA), external elastic membrane (EEM) CSA, and plaque + media (P+M) CSA. The P+M CSA were calculated as a difference between EEM CSA and lumen CSA. The cross section with the smallest lumen CSA was selected for analysis. If there were multiple cross sections with the smallest lumen CSA, the image slice with the largest EEM and P+M CSA (= the largest plaque burden) was analyzed (13,14). The identical cross section was carefully selected with intravascular or peri-vascular landmarks and a constant pullback speed (13–15). Proximal or distal reference was selected as a cross section with the largest lumen and the smallest plaque burden within 10 mm proximally and distally. Remodeling index was defined as the ratio of EEM CSA at the measured lesion (minimum luminal site) to reference EEM CSA (the average of the proximal and distal reference segments) (16). Plaque burden was calculated as: (P+M CSA/EEM CSA) × 100 (%). Interobserver variability for EEM CSA and lumen CSA were 4.3 ± 5.4% and 4.2 ± 5.1%, respectively. Intraobserver variability for EEM CSA and lumen CSA were 2.8 ± 4.9% and 2.7 ± 5.3%, respectively.

The IB-IVUS analysis was performed with previously validated, commercially available software (IB-IVUS, YD Co., Ltd.) (9). Two-dimensional (2D) color-coded maps with IB values were constructed in 21 consecutive IVUS image slices at 1-mm intervals centered at the most severe stenotic site. The quantitative IB-IVUS analysis was performed by an experienced physician unaware of the clinical data. The slices were excluded for analysis if calcification (arc >180°) was present or a side branch existed. The percentage of 4 tissue parameters under investigation (lipid pool, fibrosis, dense fibrosis, and calcification) was automatically calculated by IB-IVUS system after exact manual tracing. Because the media of coronary artery always presents a low echoic band, potentially identified with "lipid" by the current algorithm of IB-IVUS, the internal border of media (internal elastic membrane) was traced manually to eliminate the misjudgment as described in previous studies (9,17). The acoustic shadows of the guidewire and calcifications were manually traced and excluded to minimize acoustic artifacts. For 2D analysis, the cross-section of the tightest lumen was selected as the minimal lumen area (MLA) segment. Percentage lipid pool area, percentage fibrosis area, percentage dense fibrosis area, and percentage calcification area were also determined at the MLA site. After the color-coded maps were transformed into Cartesian coordinates, the percentage calcification area (calcifi-

Table 1. Patient Clinical and Lesion Characteristics (n = 56)

Male	43 (77)
Age (yrs)	68 ± 9
Clinical presentation	
Stable angina pectoris	46 (82)
Unstable angina pectoris	8 (14)
STEMI	2 (4)
NSTEMI	0 (0)
Coronary risk factors	
Hypertension	44 (79)
Hyperlipidemia	37 (66)
Diabetes mellitus	28 (50)
Smoking	17 (30)
Number of target lesions	81
Culprit lesion	48 (59)
Nonculprit lesion	33 (41)
LAD	22 (27)
LCx	15 (19)
RCA	44 (54)

Data are n (%) or mean ± SD.
LAD = left anterior descending coronary artery; LCx = left circumflex coronary artery; STEMI = ST-segment elevated myocardial infarction; NSTEMI = non–ST-segment elevated myocardial infarction; RCA = right coronary artery.

cation area/P+M CSA), the percentage dense fibrosis area (dense fibrosis area/P+M CSA), the percentage fibrosis area (fibrosis area/P+M CSA), and the percentage lipid pool area (lipid pool area/P+M CSA) were automatically counted by use of commercially available computer software (T3D, Fortner Research, Sterling, Virginia).

OCT measurements. The OCT measurements were performed at the cross sections determined by IVUS. The identical cross sections were carefully selected with intravascular and perivascular landmark and a constant pullback speed as previously reported (15). By OCT, lipid-rich plaque was defined as a signal-poor region with diffuse borders (4,8). Fibrous cap was defined as a signal-rich homogenous layer overlying the lipid-rich plaque. The OCT-derived TCFA was defined as a presence of thin fibrous cap (<65 μm) overlying a lipid-rich plaque (>90°) (8). Plaque without TCFA was defined as non-TCFA. The thinnest part of the fibrous cap was measured 3 times, and its average was defined as OCT fibrous cap thickness (18,19). All OCT images were analyzed by 2 independent investigators (T.K. and R.Y.). When there was discordance between observers, a consensus reading was obtained. Intraobserver and interobserver variability of the OCT measurements for the fibrous cap thickness were 8.8 ± 7.8% and 8.5 ± 7.3%, respectively. Intraobserver and interobserver agreements for the detection of OCT-derived TCFA were within acceptable range (intraobserver; kappa = 0.81, interobserver; kappa = 0.87, respectively).

Statistical analysis. Analysis of variance and unpaired *t* tests were used for continuous variables, and Fisher exact test was used for dichotomous variables. Data are expressed as the mean ± SD. To assess the interobserver and intraobserver variability, the results were compared with the kappa-test of concordance for the categorical data, and Bland-Altman plot was fulfilled for continuous variables. Receiver-operator characteristic (ROC) curves were constructed to determine optimal sensitivity and specificity. The association between fibrous cap thickness and plaque characteristics was investigated with linear regression. A p value <0.05 was considered statistically significant.

RESULTS

A total of 81 coronary plaques (48 culprit lesions, and 33 nonculprit lesions [nonsignificant lesion that did not require PCI]) (age 68 ± 9 years, 43 men, and 13 women) were selected from 56 patients.

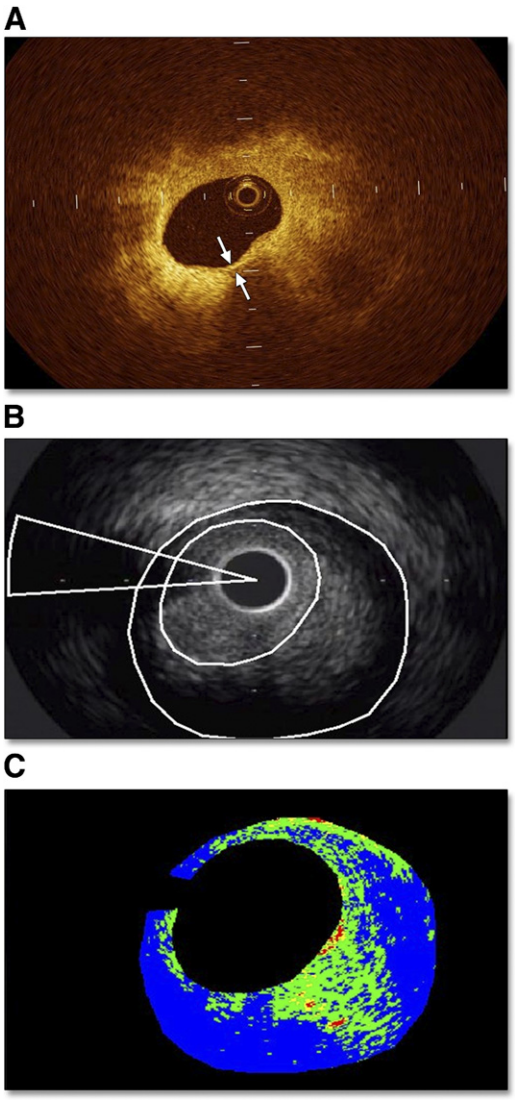

Figure 1. Representative Case of OCT-Derived TCFA OCT Image, Gray-Scale IVUS Image, and IB-IVUS Image

The fibrous cap thickness of this lesion was 50 μm by optical coherence tomography (OCT) measurement **(A) (white arrows)**, and this plaque was diagnosed as OCT-derived thin-cap fibroatheroma (TCFA). Gray-scale intravascular ultrasound (IVUS) image **(B)**. Integrated backscatter intravascular ultrasound (IB-IVUS) **(C)** revealed 40.0% percentage fibrosis area **(green)** and 56.0% percentage lipid pool area **(blue)**.

Table 1 summarizes the patient clinical and lesion characteristics. Forty plaques (49%) were classified as OCT-derived TCFA (mean fibrous cap thickness by OCT was 51.0 ± 8.4 mm), and the remaining 41 plaques (51%) were diagnosed as non-TCFA (mean fibrous cap thickness by OCT was 209.5 ± 114.0 mm). Figure 1 shows gray-scale,

JACC: CARDIOVASCULAR IMAGING, VOL. 4, NO. 6, 2011
JUNE 2011:638–46

Table 2. Lesion Characteristics

	Non-TCFA (n = 41)	TCFA (n = 40)	p Value
LAD/LCx/RCA	11/9/21	11/6/23	0.71
Reference diameter (mm)	2.70 ± 0.46	2.92 ± 0.47	<0.05
Minimal lumen diameter (mm)	1.56 ± 0.44	1.38 ± 0.52	0.10
% diameter stenosis (%)	42.2 ± 12.0	52.8 ± 14.7	<0.05
Lesion length (mm)	7.86 ± 3.38	9.36 ± 3.18	<0.05

Data are n or mean ± SD.
TCFA = thin-cap fibroatheroma; other abbreviations as in Table 1.

IB-IVUS, and OCT images from a representative case of OCT-derived TCFA.

Comparison of OCT-derived TCFA and non-TCFA. Angiographic lesion characteristics between OCT-derived TCFA and non-TCFA are summarized in Table 2. Reference diameter, lesion length, and percentage diameter stenosis of OCT-derived TCFA were significantly higher than those of non-TCFA (all $p < 0.05$). There were no significant differences in minimal lumen diameter between the 2 groups. Gray-scale IVUS and IB-IVUS results are shown in Table 3. The EEM-CSA, P+M CSA, plaque burden, and remodeling index of OCT-derived TCFA were significantly higher than those of non-TCFA (all $p < 0.05$). The IB-IVUS results demonstrated that lipid pool area was significantly larger and dense fibrosis and calcification areas were significantly smaller in the OCT-derived TCFA (all $p < 0.0001$). Similarly, percentage lipid pool area was significantly higher, and percentage calcification area, percentage dense fibrosis area, and percentage fibrosis area were significantly lower in the OCT-derived TCFA than non-TCFA (all $p < 0.0001$).

Correlation between fibrous cap thickness and IB-IVUS measurements. Correlation between fibrous cap thickness and plaque characteristics by IB-IVUS are shown in Figure 2. Percentage fibrosis area and percentage dense fibrosis area correlated positively and significantly with OCT fibrous cap thickness. Percentage calcification area correlated positively and weakly with OCT fibrous cap thickness. By contrast, percentage lipid pool area correlated negatively and significantly with OCT fibrous cap thickness.

Diagnostic values of IB-IVUS and gray-scale IVUS to classify OCT-derived TCFA. By ROC curve analysis, optimal cutoff values for the detection of OCT-derived TCFA were determined. The cutoff values of percentage fibrosis area, percentage lipid pool area, remodeling index, and plaque burden were 41%, 55%, 1.0, and 75%, respectively. Percentage lipid pool area was the best of all IVUS parameters for classifying OCT-derived TCFA (area under the curve = 0.93) (Fig. 3). Among 40 OCT-derived TCFA, 35 (88%) had a lipid area of ≥55%, whereas only 2 (5%) non-TCFA had a lipid pool area of ≥55%. Sensitivities, specificities, positive predicting values, negative predictive values, and accuracies for each parameter at the cutoffs values are shown in Table 4.

Comparison between OCT-derived and IB-IVUS-derived TCFA. With percentage lipid pool area ≥55% as an IB-IVUS criteria for detecting IB-IVUS-derived TCFA, 37 (45.7%) of 81 lesions were diagnosed as IB-IVUS–derived TCFA. Thirty-five of 37 lesions (94.6%) met both IB-IVUS and OCT criteria. Two (5.4%) of 37 IB-IVUS–derived TCFA that did not met OCT criteria for TCFA had thick-cap (≥65 μm) fibroatheroma with percentage lipid pool area ≥55%. By contrast, 5 (12.5%) of 40 OCT-derived TCFA that did not fulfill criteria for IB-derived TCFA had thin-fibrous cap but did have a small amount of percentage lipid pool area (<55%) by IB-IVUS.

DISCUSSION

Our present study demonstrated that OCT-derived TCFA had bigger vessel size, larger plaque burden, and higher remodeling index by gray-scale IVUS and had more lipid plaque and less fibrous plaque by IB-IVUS. In addition, percentage lipid pool area ≥55% was the best predictor of the OCT-derived TCFA, suggesting that IB-IVUS might be used as

Table 3. Gray-Scale and IB-IVUS Measurements

	Non-TCFA (n = 41)	TCFA (n = 40)	p value
EEM CSA (mm^2)	11.3 ± 3.4	15.8 ± 4.3	<0.0001
Lumen CSA (mm^2)	3.5 ± 1.5	4.1 ± 1.8	0.11
P+M CSA (mm^2)	7.8 ± 2.5	11.7 ± 4.1	<0.0001
Plaque burden (%)	69.2 ± 8.1	73.5 ± 10.1	<0.05
Remodeling index	0.95 ± 0.14	1.08 ± 0.15	<0.0001
% fibrosis area (%)	51.1 ± 9.5	34.7 ± 9.5	<0.0001
% dense fibrosis area (%)	7.3 ± 4.2	2.5 ± 2.0	<0.0001
% calcification area (%)	3.1 ± 2.6	0.7 ± 1.0	<0.0001
% lipid pool area (%)	38.6 ± 12.8	62.1 ± 10.8	<0.0001
Fibrosis area (mm^2)	3.92 ± 1.12	3.98 ± 1.53	0.73
Dense fibrosis area (mm^2)	0.52 ± 0.28	0.28 ± 0.22	<0.0001
Calcification area (mm^2)	0.23 ± 0.19	0.08 ± 0.11	<0.0001
Lipid pool area (mm^2)	3.18 ± 1.63	7.34 ± 3.15	<0.0001

Data are mean ± SD. Remodeling index was defined as ratio of lesion to reference external elastic membrane (EEM) cross-sectional area (CSA) (the average of the proximal and distal reference segments).
IB-IVUS = integrated backscatter intravascular ultrasound; P+M = plaque plus media; TCFA = thin-cap fibroatheroma.

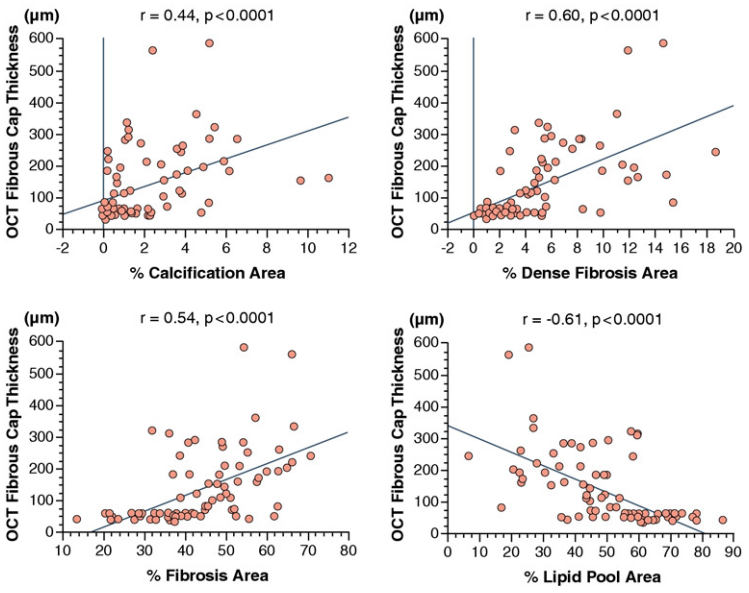

Figure 2. Correlation Between Fibrous Cap Thickness and IB-IVUS Parameters

Percentage lipid pool area correlated negatively and significantly with optical coherence tomography (OCT) fibrous cap thickness. IB-IVUS = integrated backscatter intravascular ultrasound.

an alternative or adjunctive to the OCT in detecting TCFA in vivo. Furthermore, considering that OCT alone does not provide objective and quantitative plaque characteristics of the entire vessel wall, it might be useful to combine IVUS and OCT images to further improve plaque assessments in vivo. These findings are comparable with results of not only histopathological examinations but also those from studies with another RF signal-derived IVUS system, virtual histology (VH)-IVUS (6,20). Sawada et al. (20) reported that VH-IVUS detected 28 (78%) of 36 OCT-derived TCFA with a diagnostic criteria of TCFA by VH-IVUS (6). In addition, TCFA diagnosed by both VH-IVUS and OCT had significantly larger plaque volume, vessel volume, percentage plaque volume, and vessel remodeling index, concordant with our results. Our results were also concordant with a previous clinical study to predict future ACS by IB-IVUS (21). Sano et al. (21) investigated 160 nonsignificant coronary lesions from 140 patients with angina pectoris by IB-IVUS and prospectively followed up. During follow-up (mean 30 months), 12 plaques developed ACS. By gray-scale IVUS and IB-IVUS, plaque burden, remodeling index, and percentage lipid pool area were significantly greater and percentage fibrosis area was smaller in the 12 plaques. By ROC curve analysis, optimal cutoffs of percentage fibrosis area, percentage lipid pool area, remodeling index, eccentricity rate, and plaque burden were 25%, 65%, 1.25, 0.65, and 55%, respectively (21). These cutoff values are slightly different from our present results to identify OCT-derived TCFA. One possible explanation for the discordance is a difference in the end-point (presence of OCT-derived TCFA or future ACS). Another explanation could be made by the difference in the study population. Sano et al. (21) studied only nonsignificant, nonculprit lesions, whereas we included both culprit lesions and nonculprit lesions. In addition to plaque characteristics, remodeling index was a conventional IVUS predictor of OCT-derived TCFA. This is quite concordant with the previous IVUS studies demonstrating that positive arterial remodeling is a characteristic finding of the ACS (22-24) and thus a marker of vulnerable or high-risk plaque (5,16,25-27). Our present study further demonstrated the direct correlation between plaque components and thickness of the fibrous cap. A previous study using both angioscopy and IB-IVUS demonstrated that the surface color of the plaque by angioscopy reflects the thickness of the fibrous cap determined with 2D IB-IVUS imaging (9). More recent OCT studies demonstrated that the yellowish color of the plaque by angioscopy correlates well with thickness of the fibrous cap (28,29). Our quantitative IB-IVUS results further address that thickness of the fibrous cap correlated with the total amount of lipid com-

JACC: CARDIOVASCULAR IMAGING, VOL. 4, NO. 6, 2011
JUNE 2011:638–46

Figure 3. ROC Curves for Each Intravascular Ultrasound Parameter

Receiver-operator characteristic (ROC) curves of % fibrosis area, % lipid pool area, remodeling index, and plaque burden for the classifying OCT-derived TCFA. Note that areas under the curve (AUC) show that percentage lipid pool area was the most sensitive parameter for classifying OCT-derived TCFA. Abbreviations as in Figure 1.

ponent, suggesting that both thickness of the fibrous cap and the amount of the lipid plaque could contribute to the yellowish appearance of the coronary surface by angioscopy. Previous studies demonstrated that intensive lipid lowering by statins might be efficacious for plaque stabilization/regression assessed by gray-scale IVUS as well as IB-IVUS. A recent OCT study suggested that statins might be also efficacious to prevent thinning of the fibrous cap (19). Therefore, further study with serial IVUS and OCT imaging of the nonculprit lesions with or without thin fibrous cap would possibly provide insights into interaction between fibrous cap thickness, vessel remodeling, and the amount of lipid plaque and plaque progression or stabilization in an in vivo setting (15). An improved understanding of the natural history and clinical significance of vulnerable plaques in living human patients would accelerate research in progression, treatment, and prevention of coronary artery disease.

Table 4. Diagnostic Threshold of IB-IVUS for Detecting OCT-Derived TCFA

	Sensitivity	Specificity	PPV	NPV	Accuracy
IB-IVUS					
% lipid area (cutoff ≥ 55%)	88%	93%	92%	88%	90%
% fibrous area (cutoff ≤ 41%)	85%	85%	85%	85%	85%
Gray-Scale IVUS					
Remodeling index (cutoff ≥1.0%)	85%	78%	79%	84%	82%
Plaque burden (cutoff ≥75%)	63%	61%	61%	63%	62%

IVUS = intravascular ultrasound; NPV = negative predictive value; OCT = optical coherence tomography; PPV = positive predictive value; other abbreviations as in Tables 2 and 3.

Study limitations. First, this study included relatively small numbers of patients. Therefore, these results should be confirmed by a larger study population. Second, although IB-IVUS was compared with OCT as a gold standard, we did not directly compare the results with pathology because of in vivo study design. The OCT was used to identify TCFA. Plaque component characterization errors—in particular, the differentiation of lipid and calcium—can occur, but in our study both gray-scale and IB-IVUS confirmed that no calcium was misdiagnosed as lipid in OCT-derived TCFA. However, due to OCT image artifacts, it is possible that some misinterpretation of plaque by OCT as TCFA might have occurred. Furthermore, we could observe only limited vessel areas, because the IB-IVUS and OCT procedures have several limitations for imaging certain lesions, such as severely calcified tortuous lesions or other complex lesions. Thus, our study results do not represent an unbiased sampling of all coronary arteries, and the detection rate of TCFA in our study patients might be underestimated or overestimated. Third, the natural course of the OCT-derived TCFA is still unclear and thus needs further studies. Fourth, although we investigated only TCFA as a potential cause of plaque rupture and ACS, other plaque characteristics such as plaque erosion and calcified nodule might be responsible for ACS. In addition, some selection bias was inevitable, because we selected 1 or 2 plaques in each patient. Finally, we excluded patients with severe calcified coronary plaques. Therefore, the diagnostic role of IB-IVUS for severely calcified lesions remains uncertain (30).

CONCLUSIONS

Optical coherence tomography-derived TCFA had larger plaque burden and more positive remodeling with predominant lipid component assessed by IB-IVUS.

Acknowledgments

The authors thank the research staff and nurses and technologists at the cardiac catheterization laboratories of Kawasaki Medical School Hospital. The authors also thank Dr. Hironobu Katsuyama for his professional statistical support.

Reprint requests and correspondence: Dr. Hiroyuki Okura, Kawasaki Medical School, 577 Matsushima, Kurashiki 701-0192, Japan. *E-mail: hokura@fides.dti.ne.jp.*

REFERENCES

1. Virmani R, Burke AP, Kolodgie FD, Farb A. Vulnerable plaque: the pathology of unstable coronary lesions. J Interv Cardiol 2002;15:439–46.
2. Brezinski ME, Tearney GJ, Bouma BE, et al. Imaging of coronary artery microstructure (in vitro) with optical coherence tomography. Am J Cardiol 1996;77:92–3.
3. Jang IK, Bouma BE, Kang DH, et al. Visualization of coronary atherosclerotic plaques in patients using optical coherence tomography: comparison with intravascular ultrasound. J Am Coll Cardiol 2002;39:604–9.
4. Yabushita H, Bouma BE, Houser SL, et al. Characterization of human atherosclerosis by optical coherence tomography. Circulation 2002;106:1640–5.
5. Kume T, Okura H, Kawamoto T, et al. Relationship between coronary remodeling and plaque characterization in patients without clinical evidence of coronary artery disease. Atherosclerosis 2008;197:799–805.
6. Rodriguez-Granillo GA, Garcia-Garcia HM, Mc Fadden EP, et al. In vivo intravascular ultrasound-derived thin-cap fibroatheroma detection using ultrasound radiofrequency data analysis. J Am Coll Cardiol 2005;46:2038–42.
7. Stone GW, Maehara A, Lansky AJ, et al. A prospective natural-history study of coronary atherosclerosis. N Engl J Med 2011;364:226–35.
8. Kume T, Okura H, Yamada R, et al. Frequency and spatial distribution of thin-cap fibroatheroma assessed by 3-vessel intravascular ultrasound and optical coherence tomography: an ex vivo validation and an initial in vivo feasibility study. Circ J 2009;73:1086–91.
9. Kawasaki M, Takatsu H, Noda T, et al. In vivo quantitative tissue characterization of human coronary arterial plaques by use of integrated backscatter intravascular ultrasound and comparison with angioscopic findings. Circulation 2002;105:2487–92.
10. Bridal SL, Fornes P, Bruneval P, Berger G. Parametric (integrated backscatter and attenuation) images constructed using backscattered radio frequency signals (25–56 MHz) from human aortae in vitro. Ultrasound Med Biol 1997;23:215–29.
11. Lockwood GR, Ryan LK, Hunt JW, Foster FS. Measurement of the ultrasonic properties of vascular tissues and blood from 35–65 MHz. Ultrasound Med Biol 1991;17:653–66.
12. Matsumoto D, Shite J, Shinke T, et al. Neointimal coverage of sirolimus-eluting stents at 6-month follow-up: evaluated by optical coherence tomography. Eur Heart J 2007;28:961–7.
13. Mintz GS, Popma JJ, Pichard AD, et al. Arterial remodeling after coronary angioplasty: a serial intravascular ultrasound study. Circulation 1996;94:35–43.
14. Okura H, Hayase M, Shimodozono S, Bonneau HN, Yock PG, Fitzgerald PJ. Impact of pre-interventional arterial remodeling on subsequent vessel behavior after balloon angioplasty: a serial intravascular ultrasound study. J Am Coll Cardiol 2001;38:2001–5.
15. Yamada R, Okura H, Kume T, et al. Relationship between arterial and fibrous cap remodeling: a serial three-vessel intravascular ultrasound and optical coherence tomography study. Circ Cardiovasc Interv 2010;3:484–90.
16. Okura H, Morino Y, Oshima A, et al. Preintervention arterial remodeling affects clinical outcome following stenting: an intravascular ultrasound study. J Am Coll Cardiol 2001;37:1031–5.

JACC: CARDIOVASCULAR IMAGING, VOL. 4, NO. 6, 2011
JUNE 2011:638–46

17. Kawasaki M, Ito Y, Yokoyama H, et al. Assessment of arterial medial characteristics in human carotid arteries using integrated backscatter ultrasound and its histological implications. Atherosclerosis 2005;180:145–54.
18. Kume T, Akasaka T, Kawamoto T, et al. Measurement of the thickness of the fibrous cap by optical coherence tomography. Am Heart J 2006;152:755.e1–4.
19. Takarada S, Imanishi T, Kubo T, et al. Effect of statin therapy on coronary fibrous-cap thickness in patients with acute coronary syndrome: assessment by optical coherence tomography study. Atherosclerosis 2009;202:491–7.
20. Sawada T, Shite J, Garcia-Garcia HM, et al. Feasibility of combined use of intravascular ultrasound radiofrequency data analysis and optical coherence tomography for detecting thin-cap fibroatheroma. Eur Heart J 2008;29:1136–46.
21. Sano K, Kawasaki M, Ishihara Y, et al. Assessment of vulnerable plaques causing acute coronary syndrome using integrated backscatter intravascular ultrasound. J Am Coll Cardiol 2006;47:734–41.
22. Kaji S, Akasaka T, Hozumi T, et al. Compensatory enlargement of the coronary artery in acute myocardial infarction. Am J Cardiol 2000;85:1139–41, A9.
23. Nakamura M, Nishikawa H, Mukai S, et al. Impact of coronary artery remodeling on clinical presentation of coronary artery disease: an intravascular ultrasound study. J Am Coll Cardiol 2001;37:63–9.
24. Schoenhagen P, Ziada KM, Kapadia SR, et al. Extent and direction of arterial remodeling in stable versus unstable coronary syndromes: an intravascular ultrasound study. Circulation 2000;101:598–603.
25. Varnava AM, Mills PG, Davies MJ. Relationship between coronary artery remodeling and plaque vulnerability. Circulation 2002;105:939–43.
26. Okura H, Taguchi H, Kubo T, et al. Impact of arterial remodelling and plaque rupture on target and non-target lesion revascularisation after stent implantation in patients with acute coronary syndrome: an intravascular ultrasound study. Heart 2007;93:1219–25.
27. Okura H, Kobayashi Y, Sumitsuji S, et al. Effect of culprit-lesion remodeling versus plaque rupture on three-year outcome in patients with acute coronary syndrome. Am J Cardiol 2009;103:791–5.
28. Kubo T, Imanishi T, Takarada S, et al. Implication of plaque color classification for assessing plaque vulnerability: a coronary angioscopy and optical coherence tomography investigation. J Am Coll Cardiol Intv 2008;1:74–80.
29. Takano M, Jang IK, Inami S, et al. In vivo comparison of optical coherence tomography and angioscopy for the evaluation of coronary plaque characteristics. Am J Cardiol 2008;101:471–6.
30. Kume T, Okura H, Kawamoto T, et al. Assessment of the histological characteristics of coronary arterial plaque with severe calcification. Circ J 2007;71:643–7.

Key Words: integrated backscatter intravascular ultrasound ■ optical coherence tomography ■ thin-cap fibroatheroma.